FOREX Publication
Open Access | Rapid and quality publishing

International Journal of
Electrical and Electronics Research (IJEER)
Research Article | Volume 14, Issue 2 | Pages 526-541 | e-ISSN: 2347-470X

Energy Storage System Optimal Allocation for Improving Microgrid Operation

Hager A. Elwelily[1*], Sayed H. A. El-Banna[2,3], and Mahmoud A. El-Dabah[3]

[1]Electrical Power and Machines Department, International Academy for Engineering and Media Science, Giza, Egypt; Email: hager.ashraf.sobhey@iaems.edu.eg
[2]Electrical Engineering Department, Al-Jazeera Higher Institute of Engineering and Technology, Giza, Egypt; Email: sayedelbanna@hotmail.com
[3]Electrical Engineering Department, Faculty of Engineering, Al-Azhar University, Cairo 11651, Egypt; dr_mdabah@azhar.edu.eg

***Correspondence:** *Hager A. Elwelily, hagerashrafalwelily2@gmail.com*

ABSTRACT- The rapid expansion of microgrids (MGs) is driven by the need to meet growing electricity demand sustainably through high penetration of renewable energy resources (RERs). However, the intermittency of RERs introduces significant operational uncertainty, making energy storage systems (ESSs) essential for reliable MG operation. The ESS planning problem is formulated as a constrained optimization model that incorporates power balance, battery capacity limits, and technical and operational constraints of MGs. Because it offers a viable solution, this study investigates the optimal method to allocate ESSs (batteries) using metaheuristic optimization techniques. In this work, the newly proposed Walrus Optimizer (WO) approach, which shows promising results, is used. A modified IEEE 33-bus distribution test system is employed as the benchmark. The performance of the WO is compared with five established metaheuristics: Detective Behavior Algorithm (DBA), Stochastic Social Learning Optimization (SSLO), Improved Grey Wolf Optimizer (I-GWO), Particle Swarm Optimization (PSO), and Genetic Algorithm (GA). All of these algorithms aspire to reduce power losses, boost voltage profiles, and enhance overall efficiency, reliability, stability, and operational cost reduction. Simulation results show that the WO-based framework yields a 53.56% reduction in total system power losses. Moreover, it strengthens the weakest bus voltage to 0.9803 p.u., improves the voltage stability index (VSI) to 1.0201 p.u., and accomplish a cost reduction of 10.74%, outperforming other competitive algorithms. The results demonstrate the originality and effectiveness of the WO for optimal ESS integration in RER-dominated MGs, providing an encouraging tool for enhancing voltage stability, reducing losses, and supporting reliable, sustainable, and cost-effective MG operation.

Keywords: Microgrid, Energy Storage System, Intermittency Mitigation, Voltage Profile, Power Loss, Walrus Optimizer.

ARTICLE INFORMATION

Author(s): Hager A. Elwelily, Sayed H. A. El-Banna, and Mahmoud A. El-Dabah;

Received: 02/03/26; **Accepted**: 24/05/26; **Published**: 30/06/26;
E- ISSN: 2347-470X;
Paper Id: IJEER 0203B01;
Citation: 10.37391/ijeer.140228
Webpage-link:
https://ijeer.forexjournal.co.in/archive/volume-14/ijeer-140228.html

Publisher's Note: FOREX Publication stays neutral with regard to jurisdictional claims in Published maps and institutional affiliations.

1. INTRODUCTION

Environmental pollution remains a critical global challenge, with severe implications for human health and ecosystem integrity. In this context, the widespread adoption of renewable energy resources (RERs) has become essential to reducing dependence on fossil-fuel-based power plants and mitigating greenhouse gas emissions [1]. Microgrids (MGs), which integrate distributed energy resources (DERs), energy storage systems (ESSs), and various loads, have emerged as a promising framework for enhancing system resilience and sustainability. They can operate either grid-connected or in islanded mode while delivering reliable, high-quality power to end users [2]. RERs, such as photovoltaic systems (PVs) and wind turbines (WTs), have inherently intermittent output related to their dependency on natural conditions. RERs introduce operational uncertainty and instability, despite their central role in MGs [3,4]. ESSs offer an effective solution to these challenges by smoothing power fluctuations, enhancing MG stability and reliability, and mitigating the intermittency of RERs [5]. In addition, ESSs act as supplemental reserves that help regulate daily demand variations, mitigate voltage deviations, enhance control, and reinforce overall system efficiency [6]. Despite these benefits, inadequate sizing and positioning of ESS, or overutilization in small-scale networks, may result in reduced economic returns with minimal additional advantage. Inadequate integration can elevate power losses, exacerbate frequency fluctuations, and increase both capital and operational expenses. Conversely, limited ESS capacity may lead to insufficient load support, and reliability concerns[7,8]. Therefore, optimal ESS siting and sizing are critical design tasks for modern MGs.

The sizing and planning of MGs have evolved through diverse frameworks [9]. Earliest approaches rely on simulation-based and analytical tools, such as Hybrid Optimization with Genetic Algorithm (HOGA) and the Hybrid Optimization Model for Electric Renewables (HOMER), for basic system design.

FOREX Publication
Open Access | Rapid and quality publishing
International Journal of Electrical and Electronics Research (IJEER)
Research Article | Volume 14, Issue 2 | Pages 526-541 | e-ISSN: 2347-470X

These methodologies generally utilize simplified assumptions and constrained modeling of system interactions, thus limiting their accuracy in modeling the nonlinear and coupled behavior of MGs[9,10]. Subsequently, deterministic optimization approaches were released, encompassing analytical, iterative, and numerical strategies. These methods can ensure locally optimal solutions under clearly stated assumptions. On the other hand, their practical application to MG planning issues is constrained by significant computing complexity and a lack of scaling as system capacity and decision factors increase[11-12]. In consideration of these restrictions, heuristic and metaheuristic optimization methods emerged as the leading strategy in recent literature. Algorithms like Particle Swarm Optimization (PSO) and Genetic Algorithms (GAs) are extensively utilized for their accuracy in addressing nonlinear and mixed-integer optimization challenges. Despite their uncertain characteristics and absence of assured global optimality, they offer resilient solutions for intricate MG challenges, especially in the optimal size and integration of ESSs.

Recent studies have investigated various optimization-based strategies for ESS allocation. Many studies have focused on the appropriate location of BSS while disregarding the sizing factor. Lawan et al. [13] highlighted the substantial influence of ESS on the performance of RER-based MGs and employed a Grasshopper Optimization Algorithm to determine the optimal placement of MG components, demonstrating improved performance compared with an alternative PSO-based topology. Other PSO-based approaches have been applied to radial distribution MGs to minimize energy losses by optimizing ESS placement through numerical simulations in MATLAB. These approaches often assume identical ESS units and focus primarily on loss reduction, utility cost savings, and voltage limits, while neglecting ESS scalability and detailed performance. In a modified 16-bus Witzenberg system, PSO and GA were employed to determine ESS locations that improve voltage profiles, reduce voltage violations, and minimize electricity loss costs. However, capacity planning was not considered, as ESS sizing was not explicitly addressed. In addition, the analysis primarily focused on steady-state voltage performance [14]. A two-stage planning framework was later introduced, in which a mixed-integer PSO was used to determine optimal storage locations in the first stage, followed by PSO-based daily scheduling in the second stage to reduce energy waste. Although validated on the IEEE 33-bus system under seasonal variations, this approach did not explicitly address ESS sizing, providing only partial insights into power quality and long-term planning [15]. In contrast, several studies addressed the optimal sizing of BESSs while disregarding their optimal placement. Further advances include multi-attribute grid-theory-based optimization techniques for hybrid ESS sizing, designed to account for intelligent operational characteristics and evaluate MG performance under both grid-connected and islanded modes, with the aim of balancing cost, environmental impact, and resilience [16]. A mixed-integer programming framework has also been proposed to determine optimal ESS sizing under grid-connected operation, aiming to improve MG reliability while maximizing economic benefits. The Gray Wolf Optimizer (GWO) was adopted to optimize ESS capacity and showed superior efficacy compared with GA and PSO under different scenarios, including cases with and without ESS as well as varying initial states of charge [17]. In another study, PSO combined with an innovative power management strategy was used to optimally size PV units and ESSs in a networked MG, aiming to minimize energy costs. The adopted PSO-based framework demonstrated higher accuracy and reduced computational time compared with GA [18]. Additionally, the impact of using one versus two ESS units was examined. Initial results favoring a single ESS were largely attributed to improper sizing and placement of the two-unit configuration. When both configurations were optimally designed, the two-ESS design achieved greater loss reduction. The comparative analysis indicated comparable performance between PSO and the Walrus Optimizer (WO)[19]. Representative strategies for optimal ESS sizing and placement, along with their objectives, optimization techniques, and case studies, are summarized in *table 1*.

Table 1. Summary of Previously Proposed Strategies for Optimal ESS Allocation

Ref.	Objective	Proposed Approach	Case Study	Key Characteristics
[20]	Optimal ESS allocation	Partial optimization, conventional methods, and GA	IEEE 24-bus system	GA minimized solar constraints considering power flow, enabling a robust framework comparison.
[21]	Optimal ESS capacity	PSO	Standalone MG	Considered multiple performance indices, operational costs, and battery lifespan.
[22]	Hybrid PV - WT- ESS Design	Transit Search Algorithm and PSO	Grid-connected and islanded hybrid MG	Transit Search minimized power loss and energy cost, obtaining resilient optimization.
[23]	ESS sizing and planning	Mixed-integer second-order cone programming and hybrid intelligent algorithm	IEEE 33-bus system	Incorporated demand response to maximize performance and minimize costs.
[24]	Optimal DER allocation	Hybrid GA and Intelligent Water Drops Algorithm	IEEE 33-bus and 69-bus MGs	Effectively decreased power losses and improved voltage profiles.
[25]	Optimal DG and ESS deployment	Multi-objective GWO	Unbalanced three-phase IEEE 123-bus MG	Reduced power losses and voltage unbalance.

FOREX Publication
Open Access | Rapid and quality publishing
International Journal of Electrical and Electronics Research (IJEER)
Research Article | Volume 14, Issue 2 | Pages 526-541 | e-ISSN: 2347-470X

		optimizes planning with MATLAB and OpenDSS co-simulation		
[26]	Optimal PV and ESS installation	Improved Deep Embedded Clustering algorithm integrates with K-means clustering algorithm	Improved IEEE 33-bus distribution system	Reduced voltage swings, voltages spikes at each node, and cable loss rate.
[27]	Optimal PV and ESS combination	Multi-objective non-dominated sorting genetic algorithm	Centralized PV- based energy structure	Minimized overall cost and carbon footprint.

Although numerous studies have addressed ESS sizing and, to a lesser extent, ESS placement, few works have simultaneously optimized both parameters, and most have relied on well-established optimization algorithms such as PSO and GA. Many existing approaches either treat ESS capacity as fixed, focus solely on steady-state performance, or limit the analysis to a narrow set of operating scenarios, thereby constraining their applicability to real-world MGs with high RER penetration. Most previous studies have not analyzed the influence of ESS location, capacity, and number on the peak consumption of RESs generation through optimal charge-discharge scheduling of BSSs, system stability, and cost reduction via demand shifting, as well as on identifying defective points within MGs, which may cause a collapse or failure. This gap highlights the need for a recent and robust optimization framework, as existing algorithms can be advanced yet effective in certain optimizing conditions while appearing deficient under others. Such a framework should be capable of jointly determining the optimal size, number, and location of ESS units while explicitly considering charge-discharge equilibrium and restrictions on BSSs' state of charge, along with diverse technical and operational constraints.

Thus, to address this gap, the present study develops an optimization framework based on the Walrus Optimizer (WO), a relatively recent metaheuristic, to simultaneously determine the optimal location, size, and number of ESS units in a MG. A modified IEEE 33-bus system connected to the main grid is adopted as the test MG, incorporating multiple PV and WT units as well as an ESS. The objective function is formulated to minimize power losses to significantly enhance MG operation and decrease operational costs. Power flow analysis is utilized to evaluate MG performance based on voltage profiles, voltage stability indices (VSIs) and network losses. MG performance is assessed under different ESS configurations using six optimization algorithms: WO, Improved Grey Wolf Optimizer (I-GWO), PSO, GA, and two modern methodologies, namely the Detective Behavior Algorithm (DBA) and Stochastic Social Learning Optimization (SSLO). DBA and SSLO provide capabilities such as efficient parameter adjustment, rapid convergence, robust avoidance of local optima, and adaptability across various optimization domains. Their effectiveness was evaluated in comparison with PSO and other optimization techniques[28][29] . It is hypothesized that WO, owing to its exploration–exploitation balance and search dynamics, will achieve superior MG performance compared with the benchmark algorithms. The main contributions of this work are the following:

(i) A comprehensive optimization framework that jointly addresses ESS siting, sizing, and unit number under realistic MG constraints;
(ii) A proposed framework that clearly addresses high RER penetration and fluctuating load demand profiles throughout a 24-hour operational period to optimize RER integration and boost overall MG efficiency.
(iii) A detailed performance evaluation on an MG during critical operating conditions related to the peak load demand point following RERs' integration, offering a worst-case scenario for evaluating system stability, reliability, and operational robustness within acceptable operational constraints while avoiding MG breakdowns or failures.
(iv) A different analyzed scenario assessment of ESS design, encompassing single-ESS and double-ESS allocation techniques, to evaluate the optimal scheduling organization, focusing on technical and economic evaluations through charging/discharging scheduling optimization, and operating cost reduction.
(v) A comparative evaluation of WO effectiveness for ESS planning against three widely used metaheuristics involving GA, PSO, and IGWO, as well as current advanced optimization algorithms, BDA, and SSLO, noteworthy for their rapid convergence and local optimum avoiding.

The rest of this article is organized as follows: *Section 2* begins by presenting the configuration and modeling of the tested MG system. *Section 3* subsequently addresses the ESS allocation and sizing problem, combining the objective function and operational restrictions. In *section 4*, the proposed WO-based optimization framework is introduced to effectively handle the defined problem. *Section 5* defines the initial operational settings, together with the technical specifications of the BSS, and the control parameters of the optimization methods. The simulation outcomes and performance evaluation are discussed in *section 6*, along with a comparative analysis of the obtained performance. Finally, *section 7* summarizes the main findings and outlines directions for future research.

2. TEST SYSTEM CONFIGURATION

2.1. Microgrid System

This study utilizes a modified IEEE 33-bus network configured as an MG [30]. The proposed system integrates

FOREX Publication
Open Access | Rapid and quality publishing
International Journal of Electrical and Electronics Research (IJEER)
Research Article | Volume 14, Issue 2 | Pages 526-541 | e-ISSN: 2347-470X

five PV units and four WT units, as shown in *figure 1*. *Table 2* details the specifications of the PV and WT units employed in this analysis [31].

Table 2. Specifications of Renewable Energy Resources

Bus	Photovoltaic Rating (MW)	Wind turbine Rating (MW)
5	-	1.3
8	0.5	-
12	0.4	-
18	-	1.3
21	0.5	-
24	-	1.3
28	0.5	-
31	-	1.2
33	0.4	-

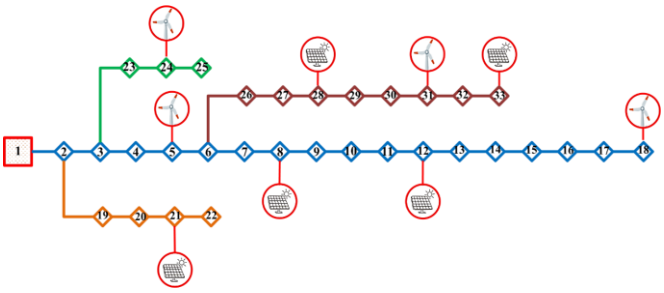

Figure 1. Modified MG Test System Under Study

2.2. Photovoltaic Mathematical Modeling

The fundamental component of a PV unit is the PV cell [32]. PV modules are formed by interconnecting these cells in series and parallel configurations [33]. *Equation (1)* defines the PV system's generated power as a function of operational conditions, demonstrating that PV performance is significantly influenced by solar radiation and temperature [34].

$$P_{PV}^{h} = N_{PV} P_{PV}^{r} \left(\frac{G}{G_0}\right)\left(1 - T_{Co}(T_{Am} - 25)\right)\eta^{inv}\eta^{rel}, \qquad (1)$$

where, P_{PV}^{h} and P_{PV}^{r} denote the generated power and the rated power of PV units, respectively. N_{PV} represents the number of PV modules. G and G_0 in (W/m²) represent the global solar irradiance and the standard solar irradiance under conventional testing conditions, respectively. T_{Co} and T_{Am} are the temperature coefficient corresponding to the PV units' maximum produced power and the ambient temperature, respectively. η^{inv} *and* η^{rel} are the inverter efficiency and the PV relative efficiency, respectively.

2.3. Wind Turbine Mathematical Modeling

The wind turbine's generated power is directly linked to the wind velocity at a specific location, as characterized by the manufacturer's power curve. This relationship is defined as a function segmented into four distinct regions, as given in *equation (2)*. Historical data from prior studies are employed to predict hourly wind speed using the Weibull distribution function [35].

$$P_{WT}^{h} = \begin{cases} 0 & v_{WT}^{h} < v_{WT}^{cut-in} \\ P_{WT}^{r}\left(\frac{(v_{WT}^{h})^3 - (v_{WT}^{cut-in})^3}{(v_{WT}^{r})^3 - (v_{WT}^{cut-in})^3}\right) & v_{WT}^{cut-in} \le v_{WT}^{h} < v_{WT}^{r} \\ P_{WT}^{r} & v_{WT}^{r} \le v_{WT}^{h} < v_{WT}^{cut-out} \\ 0 & v_{WT}^{h} \ge v_{WT}^{cut-out} \end{cases} \qquad (2)$$

where P_{WT}^{h} and P_{WT}^{r} are the WTs' generated and rated powers ; v_{WT}^{h} and v_{WT}^{r} are the hourly time step wind speed at the specific hour h and the rated speed ; v_{WT}^{cut-in} and $v_{WT}^{cut-out}$ are the WT cut-in and cut-out speeds.

2.4. Energy Storage System (ESS)

ESSs significantly impact MG stability and reliability, primarily by mitigating real and forecasted disturbances or interruption issues [36]. Among various ESS technologies (e.g., flywheel, pumped hydro), Battery Storage Systems (BSSs) are selected for this study due to their adaptability to medium-power MG requirements [37].

While battery chemistry selection depends on efficiency, lifespan, cost, and application nature, Sodium-Sulfur (NaS) batteries are identified as the most promising solution in this study. Lead-acid batteries offer low capital cost but are constrained by low efficiency (approximately 70%) and a shorter lifespan of about 7 years. Nickel-cadmium batteries provide extended lifespans (approximately 9 years) and higher efficiency (around 85%), but pose health risks due to hazardous heavy metals. Although lithium-ion (Li-ion) batteries feature rapid response, widely used, high efficiency (about 98%), and a lifespan of about 10 years, this study employed NaS over Li-ion because the optimum BSS selection depends on the application. Despite, Li-ion batteries have a higher energy density of 94–500 kWh/m³ and power density of 56.80–800 kW/m³ than NaS batteries' energy density of 150–345 kWh/m³ and power density of 1.33–50 kW/m³, lowering their mass and size. They are suitable for high-energy-density, portable, or space-limited applications like electric vehicles and electronics. For grid storage and RERs integration applications, cost-effectiveness, durability, and sustainability are prioritized over weight and dimensions. Therefore, NaS batteries provide highly reliable technology with minimal operational and maintenance expenses, offer long endurance (15 years), and achieve high efficiency (up to 90%). They also sustain extended cycle life (2,500–4,500 cycles), making them suitable for daily RER and load variation management. NaS batteries utilize affordable, accessible components, supporting economic sustainability, while lithium-ion batteries use precious, expensive minerals. Unlike Li-ion batteries, which disrupt the environment due to extraction, NaS batteries use no toxins. Thus, they are the most eco-friendly and cost-effective batteries. The downsides of NaS batteries are their high working temperatures (300–350 degrees Celsius). The ingredients' properties and need for liquid form present an issue. Thus, they require high safety.

FOREX Publication
Open Access | Rapid and quality publishing
International Journal of Electrical and Electronics Research (IJEER)
Research Article | Volume 14, Issue 2 | Pages 526-541 | e-ISSN: 2347-470X

Recent technologies use thermal insulation to maintain internal temperature and prevent heat loss. Therefore, this constraint is acceptable compared to the primary objectives of grid storage applications. NaS batteries have been widely supported in large-scale projects for demand control and RERs integration, demonstrating their development in this field [38,39].

2.5. Voltage Stability Index Modeling (VSI)

Voltage stability refers to an electrical network's capacity to maintain steady voltages within permissible limits at all buses during normal operation and disturbances. Voltage stability issues usually develop when the network is overloaded, beyond its capacity, leading to a consistent and sudden decrease in the voltage. Voltage stability indices are effective indicators for assessing voltage stability to guarantee system safety. Pinpointing essential sectors, such as lines or buses, that necessitate compensation is crucial for maintaining voltage stability and preventing overload situations. Voltage stability indices are computed for a line, a bus, or the entire network[40].A proposed voltage stability index (VSI) is derived from the transmitted reactive and active power on a distributed line corresponding to *equation (3)*. The point at which the stability index reaches its lowest level indicates the greatest susceptibility spot to voltage failure within the MG[41].

$$VSI_j = 2\mathrm{V}_i^{\,2}\,\mathrm{V}_j^{\,2} - \mathrm{V}_j^{\,2} - 2\mathrm{V}_j^{\,2}\left(P_J R_{\mathrm{IJ}} - Q_J X_{\mathrm{IJ}}\right) - |Z_{ij}|^{\,2}\left(P_J^{\,2} - Q_J^{\,2}\right), \quad (3)$$

where bus 'i' denotes the sending bus, bus 'j' denotes the receiving bus.VSI_j is VSI at the receiving spot. V_i and V_j denote the voltage of the sending and receiving nodes, respectively. P_J and Q_J represent the active and reactive power at the receiving node, respectively. Z_{ij} represents the line impedance between the sending and receiving buses.R_{IJ} and X_{IJ} denote line resistance and reactance, respectively.

2.6. The Operation Cost of the MG

The overall operational cost of MG is presented in *equation (4)*, encompassing utility operation cost (\$/kWh), WT and PV generation costs (\$/kWh), and BSS daily costs (BSDC) (\$/day)[42].

$$MG\ Operational\ Cost = \sum_{h=1}^{H}\left(B_{grid}^{h} \times P_{grid}^{h} + B_{WT}^{h} \times P_{WT}^{h} + B_{PV}^{h} \times P_{PV}^{h}\right) + BSDC, \quad (4)$$

Where h represents the hourly time step, and H denotes the 24 hour interval. P_{grid}^{h}, P_{WT}^{h}, and P_{PV}^{h} are the output powers of the grid, WT and PV at time t, respectively. B_{grid}^{h}, B_{WT}^{h}, and B_{PV}^{h} are the prevailing market energy price, and the bid prices of the WT and PV (\$/kWh) at hour *t*, respectively.

The daily cost of BSS includes the capital and replacement costs of BSS throughout the project's duration. The BSS capital cost (BSS_{cc}) is driven by its power P_{Bt} and energy capacities (E_{Bt}), as seen in the *equation (5)*.

$$BSS_{cc} = (C_P \times P_{Bt}) + (C_E \times E_{Bt}), \quad (5)$$

where C_P(\$/kW) and C_E(\$/kWh) are the particular expenses related to the power and energy capacities of the ESS.

To determine number of BSS replacements during a project's lifetime, combine *equations (6)* and *(7)* are combined to calculate the total number of cycles completed by BSS (BSS_{cycles}) .So, *equation (8)* then determine the operational lifetime of the BSS (BSS_{LT}) based on battery's life cycle ratting ($BSS_{Lifecycles}$) and the total cycle accomplished (BSS_{cycles}).

$$n_B(h,j) = \left(y_{a(i)} - y_{a(h-1)}\right)y_{a(h)}, \quad \forall \mathrm{h} \in H, \forall j \in D, \quad (6)$$

$$BSS_{cycles} = \sum_{j=1}^{D}\sum_{\mathrm{h}=1}^{H} n_B\,(h,j), \quad (7)$$

$$BSS_{LT} = \frac{BSS_{Lifecycles}}{BSS_{cycles}}, \quad (8)$$

where $n_B(h,j)$ is an indication of the cycles as a function of h and j, D signifies a total number of working days annually, that's is set at 365 in this research, and j represents the working day. $y_{a(i)}$ is a binary parameter that represents the state of the BSS during at h and j, with a y_a equal to 0 while the BSS is releasing and 1 when it is charging mode.

Therefore, The BSS replacement number BSS_{RN} over project duration (Z) is defined as indicated in *equation (9)*.

$$BSS_{RN} = \frac{Z}{BSS_{LT}}, \quad (9)$$

Thus, the $BSDC$ (\$/day) is derived using the *equation (10)*.

$$BSDC = \frac{1}{D \times Z}\left(\frac{ir(1+ir)^{Z}}{(1+ir)^{Z}-1} \times BSS_{Cc} \times BSS_{RN}\right), \quad (10)$$

where ir is the interest rate for funding BSS.

3. OPTIMAL ALLOCATION OF BSSs

3.1. Objective Function

Herein, the MG system interfaced to the primary grid was analyzed using a power flow approach to determine MG power losses and characterize the voltage profile before and after BSS optimal utilization.

The simulation results indicate the critical function of optimal BSS number, site, and sizing selection, presented by the WO and the other comparative algorithms, to fulfill the paper's objective function (OF) of minimalizing power losses over all MG Branches. Eliminating power losses investigates the MG operation related to the voltage profile and VSI, especially during peak periods, and minimizes the operational expenses for the MG. The optimization problem is formulated as a single objective function explained by *equation (11)*:

$$OF = min\sum_{B=1}^{N_B}(P_{Loss}^{B}) = min\sum_{B=1}^{N_B}(I_B^2 R_B), \quad (11)$$

FOREX Publication
Open Access | Rapid and quality publishing
International Journal of Electrical and Electronics Research (IJEER)
Research Article | Volume 14, Issue 2 | Pages 526-541 | e-ISSN: 2347-470X

where P_{Loss}^{B} expresses the active power losses of the B^{th} branch. Nb denotes the total number of MG branches; I_B is the current flowing through the B^{th} branch. R_B is the Bth resistance of the B^{th} branch.

3.2. Constraints

The BSS optimal utilization problem is subject to the following constraints.

3.2.1. Power Balance Equation

The summation of generated power from the main grid (P_{grid}^{h}), PV (P_{PV}^{h}) , WT (P_{WT}^{h}) and discharged the power of BSS ($P_{Bt}^{dis,h}$) must be equivalent to the total demand load consumption power (P_{DL}^{h}), charged power of BSS ($P_{Bt}^{ch,h}$) and MG total power losses ($P_{Loss}^{B,h}$), as represented in *equation (12).*

$$P_{PV}^{h} + P_{WT}^{h} + P_{grid}^{h} + P_{Bt}^{dis,h} = P_{DL}^{h} + P_{Bt}^{ch,h} + \sum_{B=1}^{Nb} P_{Loss}^{B,h}, \forall h \in H \quad (12)$$

where H refers to a 24-hour horizon period; h denotes a specific tested hour of the day.

3.2.2. RERs Generation Limits

The PV and WT units' generated power must be constrained within specified maximum and minimum restrictions, which cannot be exceeded, as expressed in the following *equations (13)* and *(14)*.

$$P_{WT}^{h,min} \leq P_{WT}^{h} \leq P_{WT}^{h,max}, \forall h \quad (13)$$

$$P_{PV}^{h,min} \leq P_{PV}^{h} \leq P_{PV}^{h,max}, \forall h \quad (14)$$

where $P_{WT}^{h,min}$ and $P_{WT}^{h,max}$ are the minimum and maximum generated power of the WTs, respectively. Similarly, $P_{PV}^{h,min}$, $P_{PV}^{h,max}$ indicate the PV power generation limits.

3.2.3. BSSs Limits

The BSS charging power ($P_{Bt}^{ch,h}$) and discharging power ($P_{Bt}^{dis,h}$) must be restricted to their maximum charging and discharging power limits ($P_{Bt,max}^{ch,h}$, $P_{Bt,max}^{dis,h}$) respectively ,as represented by *equations (15)* and *(16).*

$$P_{Bt}^{ch,h} \leq P_{Bt,max}^{ch,h}, \quad \forall h \leq H \quad (15)$$

$$P_{Bt}^{dis,h} \leq P_{Bt,max}^{dis,h}, \quad \forall h \leq H \quad (16)$$

Equation (17) provides the BSS state of charge SoC_h restriction at a specific hour (h) with respect to its upper and lower boundaries (SoC_h^{Max}, SoC_h^{Min}), respectively.

$$SoC_h^{Min} \leq SoC_h \leq SoC_h^{Max}, \quad \forall h \leq H \quad (17)$$

Moreover, *equation (18)* shows that the SoC_h at h is obtained based on the preceding hour SoC_{h-1} ,which is updated by adding the charged power and subtracting the discharged quantity during BSS operation. At the first hour of the day, the initial state of charge ($SoC_{initial}$) is considered. η^{Bt} and Δh represent the BSS efficiency and the time difference period, respectively, where Δh is always equal to one.

$$SoC_h = \begin{cases} SoC_{intial} + \Delta h\, \eta^{Bt}\, P_{Bt}^{ch,h} - \Delta h\ P_{Bt}^{dis,h}, & h = 1 \\ SoC_{h-1} + \Delta h\, \eta^{Bt}\, P_{Bt}^{ch,h} - \Delta h\ P_{Bt}^{dis,h}, & \forall h \geq 2, h \in H \end{cases} \quad (18)$$

Equation (19) ensures BSS operational consistency over the daily horizon by maintaining the initial and terminal states of charge at identical values.

$$SoC_{intial} = SoC_H\ , \quad (19)$$

Additionally, the total supplied power must equal the total consumed power of the BSS, accounting for its efficiency η^{Bt}, as defined in *equation (20).*

$$`\sum_{h=1}^{H} P_{Bt}^{dis,h} = \sum_{h=1}^{H} P_{Bt}^{ch,h} \times\ \eta^{Bt}, \quad (20)$$

3.2.4. Voltage Constraint

The permissible range of the Root Mean Square (RMS) voltage value at each MG busbar (i) is constrained by *equation (21)*.

$$V_{i,min} \leq V_i \leq V_{i,max}, \quad (21)$$

where $V_{i,min}$ and $V_{i,max}$ denote the upper and lower voltage limitation values, which are set at 0.95 and 1.05 p.u., respectively.

3.2.5. Branch Current Capacity Constraint

The current of each MG branch must be bounded by its upper thermal limit, as expressed in *equation (22).*

$$I_{RMS}^{B} \leq I_{RMS,max}^{B}, \quad (22)$$

where $I_{RMS}^{B}$and $I_{RMS,max}^{B}$ are the branch current flow and the branch maximum passing current capacity, respectively.

3.2.6. Load Flow Constraints

The power flow analysis technique employs two matrices: the Bus Injection to Branch Current (BIBC) matrix and the Branch Current to Bus Voltage (BCBV) matrix, making it ideal for radial distribution systems.

Equation (23) demonstrates the complex load (S_i) at each bus (i), while *equation (24)* estimates the equivalent current injection (I_i) by combining S_i and the node voltage V_i . The power flow results are obtained by repeatedly solving these equations while preserving the iteration number ($iter$)[43].

$$S_i = P_i + jQ_i \quad , \quad i = 1,2, \ldots, n \quad (23)$$

FOREX Publication
Open Access | Rapid and quality publishing
International Journal of Electrical and Electronics Research (IJEER)
Research Article | Volume 14, Issue 2 | Pages 526-541 | e-ISSN: 2347-470X

$$I_i^{iter} = \left(\frac{S_i}{V_i^{iter}}\right)^*, \quad (24)$$

$$\Delta V_i^{iter+1} + [mm] * I_i^{iter}, \quad (25)$$

$$V_i^{iter+1} + V_i^{iter} + \Delta V_i^{iter+1}, \quad (26)$$

where mm represents the multiplicative matrix of $BCBV$ and $BIBC$ matrices.

4. WO OPTIMIZATION APPROACH

Proposed by Pavel et al. [44] in 2022, WO is a novel bio-inspired metaheuristic algorithm. This optimization algorithm mimics walrus behavior in its native environment, including harvesting and adaptation strategies. The foraging behavior of walruses enables extensive exploration of diverse candidate solutions, enhancing the ability to evaluate all options and optimize outcomes effectively.

The WO has gained significant interest in power system and MG applications according to its efficient global search ability and balancing exploration–exploitation dynamics. Modern MGs with significant integration of RERs are fundamentally defined by unpredictable generation, fluctuating power flow, and strong interactions with voltage stability and demand flow, leading to a highly nonlinear and complex coupled dynamic system[45]. WO was tested using 68 benchmark functions and compared with 10 notable metaheuristic methods. The outcomes reveal that WO is highly competitive with other algorithms and yields the most effective solutions to optimization challenges. WO demonstrates competitive performance relative to PSO, GWO, and other hybrid evolutionary and swarm-based techniques, particularly regarding convergence speed, solution quality, and robustness in uncertain conditions. Additionally, WO derives the optimal solution from the proposed solution group based on walrus flexibility and behavioral intelligence Moreover, WO highly suitable for real-time and adaptive energy management[46]. Recent research indicates that WO-based solutions are notably effective in improving the functioning of the distribution system, optimizing power flow, and tackling MG energy administration and RER integration challenges, resulting in enhanced convergence characteristics and more cost-effective dispatch strategies [47]. The WO methodology depends on three stages: initialization, migration, and exploitation. The WO framework steps are as follows: initialization, objective function estimation, feeding and foraging, migration, exploitation, and termination.

4.1. Algorithm Initialization

In WO, walruses are regarded as population members that are randomly organized within a population matrix, as defined mathematically by *equation (27).* Each walrus represents a potential solution to the optimization problem, and its location in the search domain indicates the feasible ranges of the associated parameters. As a result, each one in this group's array can be an integer.

$$X = \begin{bmatrix} X_1 \\ \vdots \\ X_i \\ \vdots \\ X_N \end{bmatrix}_{W\times m} = \begin{bmatrix} x_{1,1} & .. & x_{1,j} & .. & x_{1,m} \\ \vdots & \vdots & \vdots & \vdots & \vdots \\ x_{i,1} & .. & x_{i,j} & .. & x_{i,m} \\ \vdots & \vdots & \vdots & \vdots & \vdots \\ x_{N,1} & .. & x_{N,j} & .. & x_{N,m} \end{bmatrix}_{N\times m}, \quad (27)$$

where X represents the population of walrus; X_i denotes the candidate option of the i^{th} Walrus; $x_{i,j}$ indicates the selected value of the j^{th} choice parameter associated with i^{th} walrus; N denotes the total population count; m represents the number of decision parameters.

4.2. Objective Function Estimation

The primary objective determines the optimal solution, which is derived from the values given in *equation (28).*

$$OF = \begin{bmatrix} OF_1 \\ \vdots \\ OF_i \\ \vdots \\ OF_N \end{bmatrix}_{N\times 1} = \begin{bmatrix} OF(X_1) \\ \vdots \\ OF(X_i) \\ \vdots \\ OF(X_N) \end{bmatrix}_{N\times 1}, \quad (28)$$

where OF represents the objective function array and OF_i denotes the objective value corresponding to the i^{th} walrus. The walrus achieving the best assessed objective value is considered the ideal candidate solution.

4.3. The Feeding and Foraging Process

Within the walrus population, long-tusked individuals influence other members by guiding them toward high-quality feeding sites. In this step, the walrus's (i^{th}) updated position ($x_{i,PO1}$)is computed according to *equation (29)*, and the corresponding objective function value ($OF_{i,PO1}$) is evaluated. Whenever the modified position yields a better objective value, it replaces the previous one; otherwise, the original position (x_i) is retained, as described in *equation (30).*

$$x_{(i,j),PO1} = x_{(i,j)} + rand_{(i,j)}\left(SW_j - I_{(i,j)} \cdot x_{(i,j)}\right), \quad (29)$$

$$x_i = \begin{cases} x_{i,PO1} & , OF_{i,PO1} < OF_i \\ x_i & , else \end{cases} \quad (30)$$

where $x_{ij,PO1}$ represents the j^{th} dimension of the i^{th} updated position, $rand_{(i,j)}$denotes randomly generated values in the interval [0, 1], while SW refers to the best solution corresponding to the optimal objective value, and $I_{(i,j)}$ represents randomly selected integers within the range (1 to 2).

4.4. Migration Process

Walruses move to rocky or sandy coastlines when the weather heats up at the end of summer. This migration behavior is intended to guide walruses as they explore the region in search of suitable spots. It reflects a mechanism in which each walrus moves to a random position within the search domain. As a result, an alternative suggested location $x_{i,PO2}$ is initially calculated using the *equation (31).* As described in *equation (32)*, whenever a new position improves the desired functional

FOREX Publication
Open Access | Rapid and quality publishing
International Journal of Electrical and Electronics Research (IJEER)
Research Article | Volume 14, Issue 2 | Pages 526-541 | e-ISSN: 2347-470X

objective, it replaces the walrus's previous position. otherwise, the original position (x_i) is retained.

$$x_i = \begin{cases} x_{(i,j)} + rand_{(i,j)} \cdot \left(x_{(C,j)} - I_{(i,j)} \cdot x_{(i,j)}\right) & , OF_C < OF_i \\ x_{(i,j)} + rand_{(i,j)} \cdot \left(x_{(i,j)} - x_{(C,j)}\right) & , else \end{cases} \quad (31)$$

$$x_i = \begin{cases} x_{i,PO2} & , OF_{i,PO2} < OF_i \\ x_i & , else \end{cases} \quad (32)$$

where $x_{(i,j),PO2}$ is the j^{th} dimension of the i^{th} new position; $OF_{i,PO2}$ represents its calculated functional objective ; $C \in \{1,2,\ldots..,N\}$, and $C \neq i$ provides the new selected position that the i^{th} walrus will move to ; $x_{(C,j)}$ denotes its j^{th} vector; OF_C represents its evaluated functional objective.

4.5. Escaping and Fighting Against Predators (Exploitation)

Walruses are constantly at risk from predators such as polar bears and killer whales. Their escape and defensive strategies lead to changes in their positions within their immediate surroundings. By simulating this natural behavior, the WO enhances its exploitation capability during local searches in the solution area around suggested options. To model this phenomenon, each walrus is assumed to be surrounded by its vicinity. An updated position $x_{i,PO3}$is generated inside this vicinity utilizing *equations (33)* and *(34)*. Once the updated position improves the desired objective, it replaces the previous one; otherwise, the original position (Xi) is retained according to *equation (35)*.

$$x_{(i,j),PO3} = x_{(i,j)} + (lc_{local,j,T} + (uc_{local,j,T} - rand_{(i,j)}\, lc_{local,j,T})), \quad (33)$$

$$Local\ constraints = \begin{cases} lc_{local,j,T} = lc_j\ /T\ , \\ uc_{local,j,T} = uc_j\ /T \end{cases} \quad (34)$$

$$x_i = \begin{cases} x_{i,PO3} & , OF_{i,PO3} < OF_i \\ x_i & , else \end{cases} \quad (35)$$

where $x_{(i,j),PO3}$ is the j^{th} dimension of the i^{th} new location; $OF_{i,PO3}$ denotes its evaluated objective value;Tindicates the repetition contour; lc_j and uc_j represent the lower and upper constraints of the j^{th} parameter, respectively; and $lc_{local,j,T}$ and $uc_{local,j,T}$ provide the local lower and upper constraints associated with the j^{th} parameter, respectively, enabling the search within the surrounding area for potential alternatives.

4.6. Termination Criteria

The algorithm terminates upon reaching the maximum number of iterations or when a sufficiently low objective function value is obtained. Otherwise, the process returns to the objective function estimation step. *Figure 2* displays the WO framework flowchart. Finally, the algorithm outputs the best solution along with relevant performance metrics, such as convergence behavior and computational efficiency, while maintaining a balance between exploration and exploitation. This provides insights into WO productivity and ensures effective global search while avoiding premature convergence. Simulations were conducted using MATLAB R2021b on a laptop with an Intel® Core™ i7-8850H CPU @ 2.60 GHz and (2.59 GHz), and 16.00 GB RAM. The WO parameters were set to 100 iterations and a population size of 10.

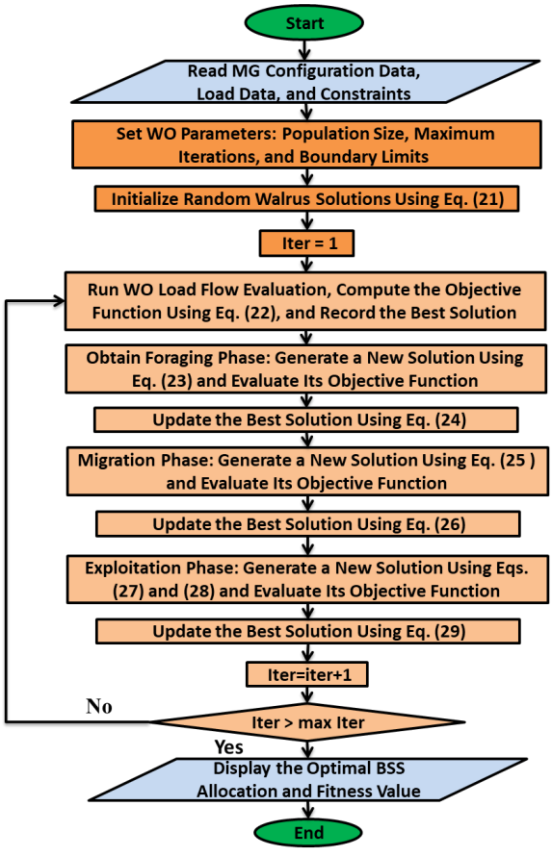

Figure 2. Flowchart of the WO Algorithm Phases

5. DATASETS

This study investigates a grid-connected MG comprising five PV units, four WT units, and multiple loads, as shown in *figure 3*. The locations and ratings of the RER units are summarized in *table 2*. The RERs are integrated to track the variable load demand over a 24-hour period and thereby enhance operational reliability. *Figure 3* illustrates the hourly load profile and corresponding RER output, from which three main operational challenges are identified.

First, during off-peak hours from hour 3 to hour 7, RER generation exceeds load demand, creating surplus power that an ESS must absorb. Ensuring an appropriate balance between daily RER production and consumption is therefore essential. Second, during peak hours (around hour 16 and from hour 18 to hour 21), load demand exceeds RER generation, leading to overloading conditions and voltage deviations across several buses. To alleviate these overloads, a BSS is introduced to discharge stored energy during peak periods while satisfying predefined power-balancing criteria. Third, power flow analysis reveals that the system exhibits unacceptably high-

FOREX Publication
Open Access | Rapid and quality publishing
International Journal of Electrical and Electronics Research (IJEER)
Research Article | Volume 14, Issue 2 | Pages 526-541 | e-ISSN: 2347-470X

power losses, highlighting the need for optimal BSS siting and sizing within the MG. To address these issues, Sodium–Sulfur (NaS) batteries are adopted as the BSS technology, as shown in *table 3*. The battery SoC is initialized at 0.3 of its rated capacity and constrained between 0.1 and 0.9 to preserve battery life and ensure stable operation, in accordance with Institute of Electrical and Electronics Engineers (IEEE) recommendations [48]. These modeling assumptions provide a consistent basis for comparing the six proposed optimization algorithms, each of which yields a distinct solution for BSS design and allocation, enabling an objective performance assessment. *Table 4* details the control parameters for the optimizers. For instance, Population-based algorithms such as WO can achieve steady convergence with relatively small populations due to their inherent search dynamics and balanced exploration-exploitation characteristics. The population size was established at 10, and the maximum number of iterations was constrained to 100 for computational efficiency. An increase in population size does not intrinsically improve solution quality; it significantly raises computing costs. Similarly, 100 iterations were considered sufficient for achieving near-optimal convergence. The residual parameters, encompassing the convergence control parameter, migration, risk, and clustering-related parameters, are adaptively modified throughout the search process. These parameters govern population variety, improve global search, and prevent premature convergence[49].

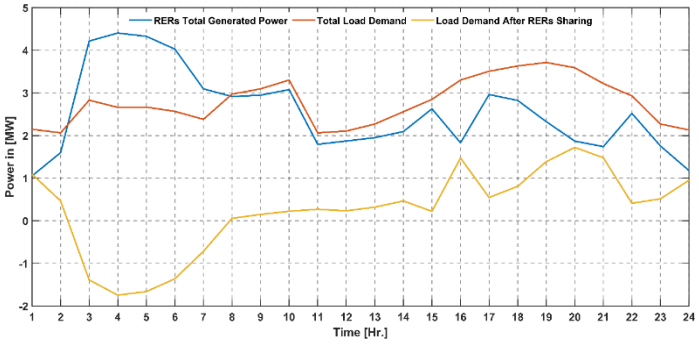

Figure 3. The Total Demand Load and the Total RERs Output Power per Hour

Table 3. NaS Battery Parameters

Parameter	Values
Initial SoC	0.3
Minimum SoC	0.1
Maximum SoC	0.9
Efficiency (%)	90
Span time(years)	15

Table 4. Control Parameters of the proposed Optimizers [50- 52].

Algorithm	Population Size	Iterations	Key Parameters
WO	10	100	Convergence parameter (α:1→ 0), risk factors (A , R), migration factor (β), distress coefficient (P), clustering coefficients (a , b)
DBA	10	100	Motion control parameter (α=0.5), investigation and attack Probability (P_{invest} = 0.5, P_{attack} = 0.5)
I-GWO	10	100	Convergence parameter (a:2→ 0), enclosing and displacement coefficient vectors (A, C)
SSLO	10	100	Social and balance learning criteria ($\alpha = 1,\ \beta = 0.5$)
PSO	10	100	Inertia weights ($\omega_{max} = 0.9$, $\omega_{min} = 0.2$), acceleration coefficient ($c_1 = 1$, $c_2 = 2$)
GA	10	100	Crossover and mutation probabilities ($P_c = 0.95, P_m = 0.001$)

6. RESULTS EVALUATIONS AND DISCUSSION

The optimization process is investigated during the critical peak load hour (hour 20), when the load reaches 1.7 MW following the inclusion of RERs, as illustrated by the load variations in *figure 3*, representing the most critical MG operating condition. Six optimization algorithms are employed: WO, DBA, I-GWO, SSLO, PSO, and GA. The primary objective is to determine the optimal number, size, and location of BSS units within the MG to enhance the voltage profile, improve voltage stability, and reduce power losses. Table 5 presents the MG performance for the different BSS designs obtained by all algorithms through power flow analysis under system constraints. The table evaluates MG performance in terms of the minimum voltage value, the lowest VSI at the weakest bus (Bus 33), and the MG losses during the optimization hour, which represent the objective function value for each scenario. In addition, the table summarizes three operating scenarios: without BSS, with a single optimally allocated BSS, and with two optimally allocated BSS units, as follows.

6.1. Microgrid Performance Without BSS

This study examined the worst-case MG operating scenario to identify the maximum per-unit (p.u.) bus voltage drop at Bus 33 and the highest total power losses. The minimum p.u. voltage and VSI are 0.9295 and 0.9612, respectively, while the total power loss reaches 92.59 kW. The baseline scenario, which consists solely of RER generation without BSS interaction, exhibits the highest power losses and therefore serves as a reference case for evaluating the benefits of BSS integration. These results highlight the necessity of optimal BSS allocation within the MG.

6.2. Microgrid Performance With Single BSS

GA and PSO optimized 1 MW BSS configurations at Buses 10 and 29, respectively. These configurations achieved loss reductions of 11.95% and 17.59%, and improved the minimum p.u. voltage to 0.952339 and 0.9562, with VSI values of 0.97904 and 0.98111, respectively. The DBA and SSLO provided results identical to those of PSO. In contrast, WO

FOREX Publication
Open Access | Rapid and quality publishing
International Journal of Electrical and Electronics Research (IJEER)
Research Article | Volume 14, Issue 2 | Pages 526-541 | e-ISSN: 2347-470X

and I-GWO optimized a 1.5 MW BSS configuration at Bus 6, reducing overall losses by 40.91% while improving the minimum p.u. voltage and VSI to 0.964111 and 1.001716, respectively. The outstanding performance of WO demonstrates its advanced ability for achieving optimal power distribution under MG operating constraints compared to the other approaches.

6.3. Microgrid Performance With Two BSS Units

This case demonstrated clear performance differences among the six optimizers. For example, GA proposes two BSS units: 0.5 MW at Bus 4 and 0.4 MW at Bus 11, reducing overall power losses by 18.10% and improving the weakest p.u. voltage and VSI to 0.95633 and 0.982329, respectively. Similarly, all algorithms indicate two batteries with different configurations and results provided in the table, further highlighting the differences among the methods and indicating the superior performance of the WO optimizer. WO achieves optimal operational performance by selecting two BSS units: 1.3 MW at Bus 29 and 1 MW at Bus 2. This configuration achieves a loss reduction of 53.56%, representing the highest reduction level, while improving the minimum p.u. voltage and VSI to 0.9803 and 1.0201, respectively. The findings confirm the effectiveness of WO due to its improved MG performance and loss reduction, which also leads to cost reduction, demonstrating higher efficiency compared to the other optimizers.

Table 5. MG Performance Comparison Based on the Optimal Allocation of BSSs Using Proposed Optimizers

Case	Optimizer	Location Bus	Size (MW)	Capacity (MWh)	Min. Voltage (p.u.)	Min. VSI (p.u.)	Total Losses (KW)	Losses Reduction (%)
W/O BSS	–	–	–	–	0.9295	0.9612	92.59	-
1 BSS	WO and I-GWO	6	1.5	5.5	0.9641	1.002	54.71	40.91
	PSO&DBA& SSLO	29	1	5	0.9562	0.9811	76.3	17.59
	GA	10	1	5	0.9523	0.979	81.53	11.95
2 BSS	WO	29	1.3	4	0.9803	1.0201	43	53.56
		2	1	6				
	DBA	17	0.2	1	0.9783	1.0161	51.81	44.04
		30	1	5				
	I-GWO	16	0.2	1	0.9772	1.0149	52.18	43.64
		29	1	5				
	SSLO	30	1	5	0.9679	1.0027	66.74	27.91
		1	0.1	0.5				
	PSO	27	0.2	1	0.9585	0.9903	74.08	19.99
		9	0.6	3				
	GA	4	0.5	2.5	0.9563	0.9823	75.83	18.10
		11	0.4	1.8				

To guarantee the reliability of the results, all optimization procedures were performed 10 times during loss mitigation. This supports a rigorous statistical assessment of solution quality and reproducibility. *Table 6* presents the maximum, minimum, and average loss reductions for the six employed optimization methods. These reductions represent the main performance indicator investigated in this study. In addition, the values of the standard deviation (std) are provided to evaluate the consistency and stability of the obtained results.

As observed from the table, WO demonstrated superior performance compared to the other algorithms, achieving the highest loss reduction of 0.0430 MW, while DBA followed with consistent, although comparatively lower, improvements. I-GWO also exhibited stable, albeit with slightly lower improvements than DBA. This was followed by SSLO, PSO, and finally GA, which, despite still outperforming the baseline case without BSS, showed the lowest improvement and higher variability.

Regarding result consistency, all employed optimizers produced relatively small deviations and stable convergence behavior, except for GA. Notably, WO remained particularly effective, as it achieved both the best objective value and an almost negligible standard deviation, as illustrated in *figure 4*. These results confirm the strong consistency of WO and validate its suitability for MG applications.

FOREX Publication
Open Access | Rapid and quality publishing
International Journal of Electrical and Electronics Research (IJEER)
Research Article | Volume 14, Issue 2 | Pages 526-541 | e-ISSN: 2347-470X

Table 6. Performance Indicators of the Proposed Optimization Algorithms for the Double-BSS Configuration

Index/ Algorithm	GA	PSO	SSLO	I-GWO	DBA	WO
Best	0.0758	0.07408	0.06674	0.0522	0.0518	0.0430
Worst	0.0804	0.07409	0.06674	0.0525	0.0519	0.0430
Mean	0.0783	0.0741	0.06674	0.0523	0.05184	0.0430
std%	1.8647	0.0029	0.000164	0.21981	0.0778	0.0067

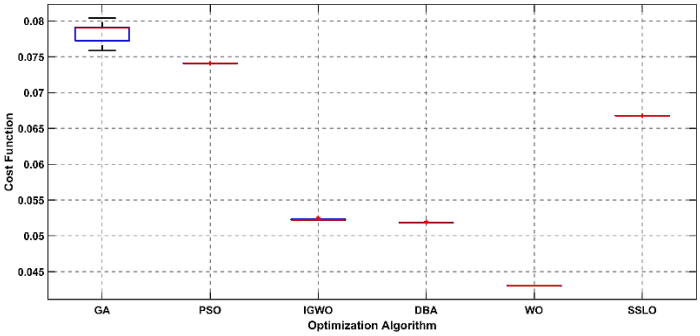

Figure 4. Box Plot Analysis of the Proposed Algorithm for the Double BSS Configuration

The total power losses and voltage profile were analyzed for each hourly interval in all study cases, both before and after optimal BSS integration. For instance, *Figure 5* illustrates MG total power-loss mitigation during peak load hours using the double BSS configurations from the six optimizers. This figure clearly indicates that, during all peak hours, WO reduced MG losses by nearly 50% of the base scenario, illustrating its outstanding loss mitigation efficacy. For example, at hour 21 the WO double BSS design achieved MG losses of 41.5 MW, while the MG losses without BSS were 78.3 MW, indicating a power saving of 47%.

To demonstrate the double BSS designs employing GA, PSO, SSLO, I-GWO, DBA, and WO integration for enhancing the MG voltage profile during peak load hours, *Figures 6* and *7* depict the voltage profiles at hours 19 and 20, corresponding to 97% and 100% of the maximum load requirement after the integration of RERs, as indicated by the daily load profile in *figure 3*. *Figures 6* and *7* clearly indicate that the voltage profile of the MG improved compared to the baseline scenario without BSS, since the BSS discharged during these hours, facilitating regulating the voltage of those high loads. Also, *figure 8* illustrates the voltage profile at hour 11 (16% loading following the integration of RERs). It is noteworthy that the voltage profile of the MG remains consistent throughout all scenarios, as the voltage remains stable outside of the BSS charging and discharging intervals, signifying restricted storage impact under low-load conditions. Meanwhile, *Figure 9* demonstrates the MG voltage profile at hour 5, suggesting a negative loading percentage related to RER surplus power.

The voltage profile of the MG without an integrated BSS reaches its maximum levels, indicating overvoltage tendency. After BSS integration into the MG, the BSS is charged due to excess power and low market price. Therefore, the MG voltage profile decreases from the base case due to the absorption of excess generation. Although the voltage lower limit was not violated in any situation, the WO double design produced voltage values closest to the base case when compared to the other double designs, indicating superior performance.

Figures 10 and *11* illustrate the impact of BSS on the VSI during peak load hours 19 and 20 respectively, in line with the voltage improvements shown in *figures 6* and *7*. The results indicate that MG stability is enhanced through increased VSI values compared to the baseline without BSS, under GA, PSO, SSLO, I-GWO, DBA, and WO double BSS configurations, confirming the superior performance of the WO design. Moreover, *figure 12* shows a reduction in VSI during off-peak hour 5, corresponding to the deterioration in the voltage profile in *figure 8*, with WO maintaining values closest to the base case.

Moreover, *figure 13* shows the fitness value on the *y*-axis versus the number of epochs on the *x*-axis, with six curves representing the convergence characteristics of GA, PSO, SSLO, I-GWO, DBA, and WO within the MG after expanding the system to include single BSS configurations. The GA approach starts with a relatively high fitness value of around 0.100523 MW. As the iterations progress, the GA algorithm reduces the fitness value, which stabilizes at approximately 0.08153 MW after about 15 iterations. The PSO, SSLO, and DBA approaches provide moderate improvements in convergence, achieving optimal values of 0.07630 MW after 21, 15, and 6 iterations, respectively. The I-GWO and WO strategies converge rapidly to low fitness levels, stabilizing at approximately 0.0547 MW after 8 and 6 iterations, respectively. *Figure 14* demonstrates the comparative performance of these six algorithms within the MG under double BSS configurations, with the GA algorithm initiating at a maximum fitness value of 0.0760 MW. Over time, the GA algorithm decreases the fitness value, eventually settling at 0.0758 MW after 42 iterations. The PSO algorithm follows, reaching a plateau at a slightly lower fitness level than GA and maintaining a value of 0.0741 MW after 8 iterations. The SSLO algorithm demonstrates moderate convergence among all techniques, stabilizing at around 0.0066 MW after 22 iterations. Although DBA starts with a higher fitness value than I-GWO, it stabilizes at 0.05182 MW after 10 iterations, while I-GWO remains constant at 0.01521 MW after 66 iterations. The results indicate that WO converges from 0.0432 MW to an optimal solution of 0.0043 MW after 15 iterations, outperforming the alternative methods and demonstrating superior fitness performance. These results further confirm that WO significantly enhances optimization efficiency.

FOREX Publication
Open Access | Rapid and quality publishing
International Journal of Electrical and Electronics Research (IJEER)
Research Article | Volume 14, Issue 2 | Pages 526-541 | e-ISSN: 2347-470X

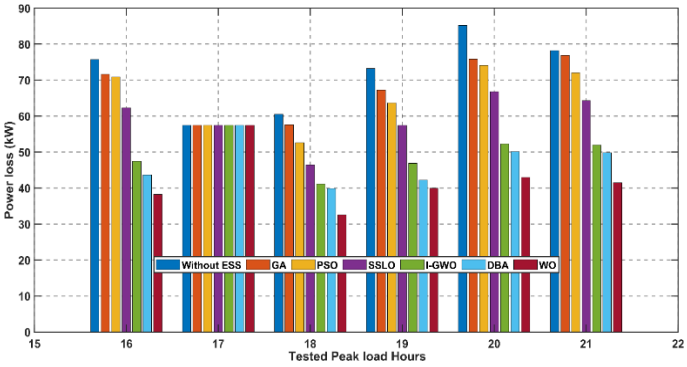

Figure 5. Power Losses During Peak Hours for Different Double BSS Designs

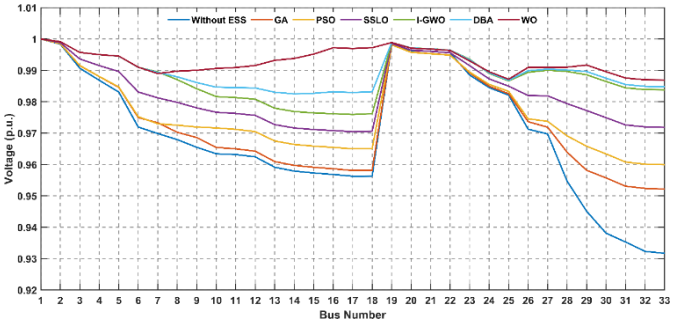

Figure 6. Voltage Profile Analysis of the MG under Different Double BSS Designs at Hour 19

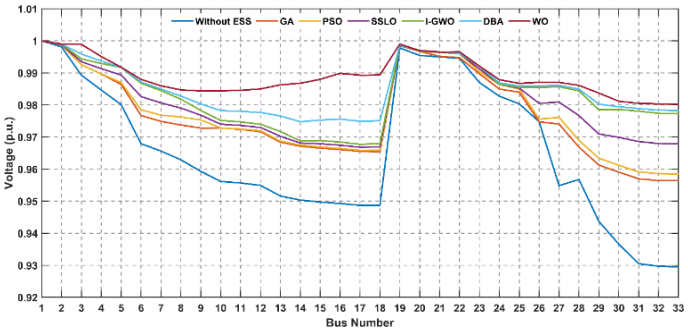

Figure 7. Voltage Profile Analysis of the MG under Different Double BSS Designs at Hour 20

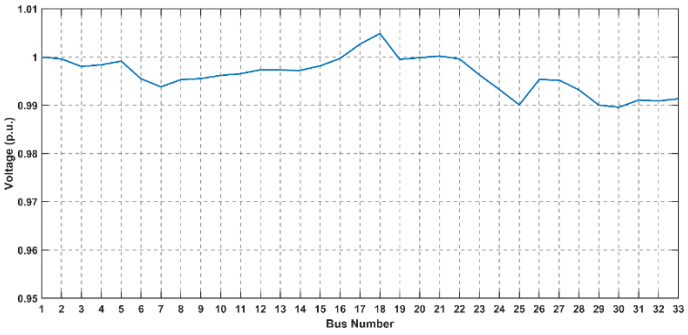

Figure 8. Voltage Profile Analysis of the MG under Different Double BSS Designs at Hour 11

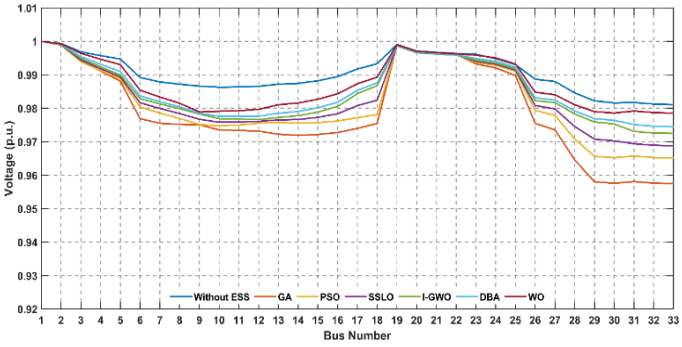

Figure 9. Voltage Profile Analysis of the MG under Different Double BSS Designs at Hour 5

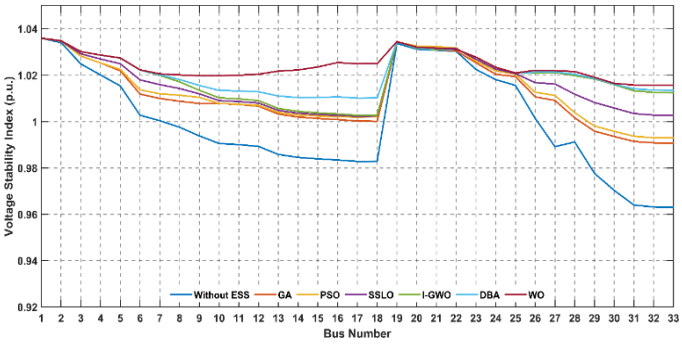

Figure 10. Assessment of Voltage Stability Index under No BSS and Double BSS Configurations at Hour 19

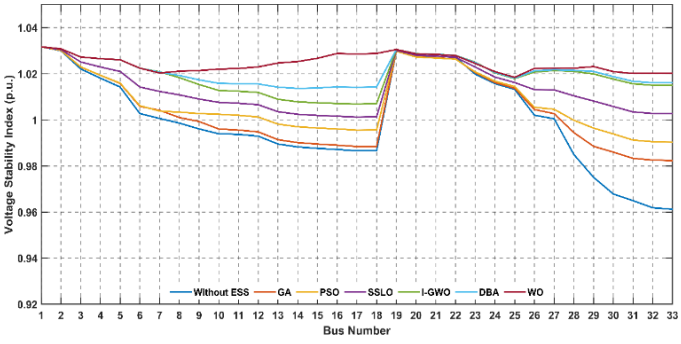

Figure 11. Assessment of Voltage Stability Index under No BSS and Double BSS Configurations at Hour 20

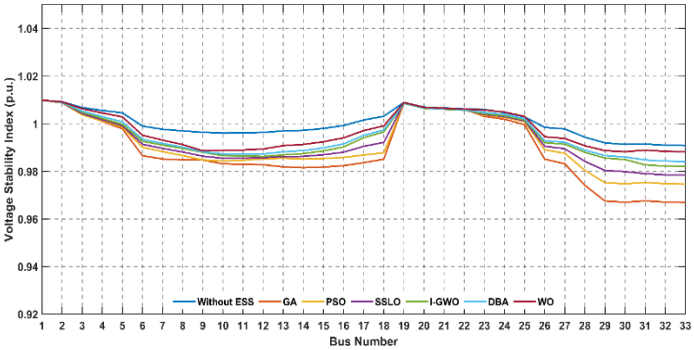

Figure 12. Assessment of Voltage Stability Index under No BSS and Double BSS Configurations at Hour 5

FOREX Publication
Open Access | Rapid and quality publishing
International Journal of Electrical and Electronics Research (IJEER)
Research Article | Volume 14, Issue 2 | Pages 526-541 | e-ISSN: 2347-470X

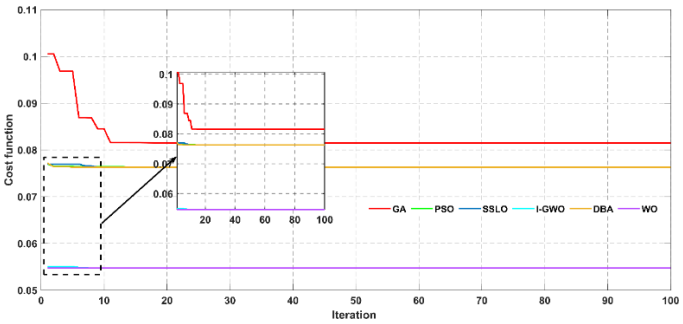

Figure 13. Convergence Characteristics of WO, DBA, I-GWO, SSLO, PSO and GA for Single BSS Designs

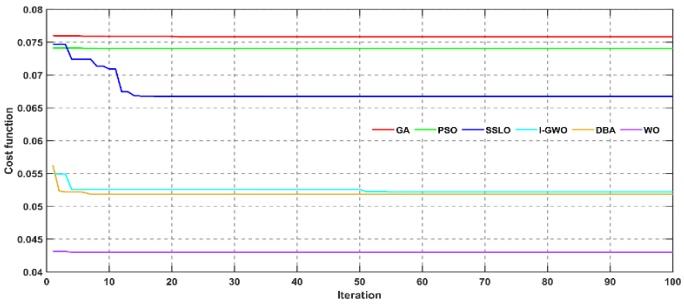

Figure 14. Convergence Characteristics of WO, DBA, I-GWO, SSLO, PSO and GA for Double BSS Designs

To assess the economic impact of the BSSs on system performance, the operating cost of the MG is analyzed under different operating conditions. *Table 7* presents the bidding prices of the PV and WT units, together with the cost parameters of the NaS batteries employed in this study. Furthermore, the electricity market price exhibits considerable fluctuations, fluctuating significantly between off-peak and peak-demand periods. Such variations emphasize the economic significance of the BSSs in reducing the MG operating cost by effective energy management and enhanced utilization of RERs, hence improving MG economic performance of the system.

Table 7. PV and WT Bidding Prices and NaS Battery Cost Parameters[42].

Item	value
PV Bid ($/kWh)	2.8
WT Bid ($/kWh)	1.72
Grid Bid ($/kWh)	Time Varying
NaS Capital Cost of Power ($/kW)	350
NaS Capital Cost of Energy ($/kWh)	300

Table 8 presents the computed operating costs of the MG with and without BSS interaction, including grid, PV, WT, BSS capital, total BSS daily costs, and the overall daily operating cost. In the base case, the operating cost accounts for MG operation and power losses. The BSS daily cost includes capital and replacement costs over a 35-year project lifetime, with an interest rate of 0.02 considered to guarantee a realistic economic analysis. The NaS battery lifecycle is adopted from *table 3*, while the annual number of cycles BSS_{cycles} and lifetimeBSS_{LT} are used to determine the required replacements BSS_{RN} over the project horizon. The percentage cost reduction is evaluated relative to the base case.

The findings indicate that the MG running cost is significantly reduced by the optimal BSS design. *Table 5* clearly indicates that the case corresponding to the implementation of the WO algorithm yields the highest percentage of savings in operating costs (10.74%). This is due to its optimal power distribution between the storage units and the grid, along with a substantial reduction in power losses, which consequently reduces grid operating costs, especially during peak-load periods when energy market prices are high.

Figure 15 illustrates the optimal output power of the grid, PV, WT, and the WO double BSS for each hour of the day. Furthermore, based on daily load and generation profiles, power flow constraints, and balancing requirements, the BSS charging and discharging power is calculated hourly as a function of the SoC levels. *Figure 16* illustrates the SoC of the WO double BSS at each hour of the day. It indicates that both BSS units are charged from hour 3 to hour 7 during periods of surplus power and low market prices. Following full charging, the BSS units discharge when the total generation is insufficient to satisfy MG technical performance requirements and when energy market prices are high, thereby reducing operational costs and enhancing system performance during peak hours.

Table 8. MG Operational Cost Comparison with and without Double BSS configurations Using Proposed Optimization Algorithms

Case	Operation cost ($)	BSS capital cost ($)	BSS_{RN}	BSS cost/day ($/day)	Total BSS cost /day ($/day)	Total operating cost/day ($/day)	Saving (%)
W/BSS	142681.54	-----	-----	-----	-----	142681.54	-----
Two BSS (WO)	124439.49	6389310.16	3	1633.89	2920.16	127359.65	10.74
		5029969.32	3	1286.27			
Two BSS (DPA)	129109.14	5029969.32	3	1286.27	1543.53	130652.67	8.43
		1005993.86	3	257.25			
Two BSS (I-GWO)	128368.62	5029969.32	3	1286.27	1543.53	129912.15	8.95
		1005993.86	3	257.25			
Two BSS (SSLO)	131470.86	5029969.32	3	1286.27	1414.90	132885.76	6.87
		502996.93	3	128.63			
Two BSS (PSO)	133040.90	3017981.59	3	771.76	1029.02	134069.92	6.04
		1005993.86	3	257.25			
Two BSS (GA)	133307.00	2514984.66	3	643.14	1157.65	134464.64	5.76
		2011987.73	3	514.51			

FOREX Publication
Open Access | Rapid and quality publishing
International Journal of Electrical and Electronics Research (IJEER)
Research Article | Volume 14, Issue 2 | Pages 526-541 | e-ISSN: 2347-470X

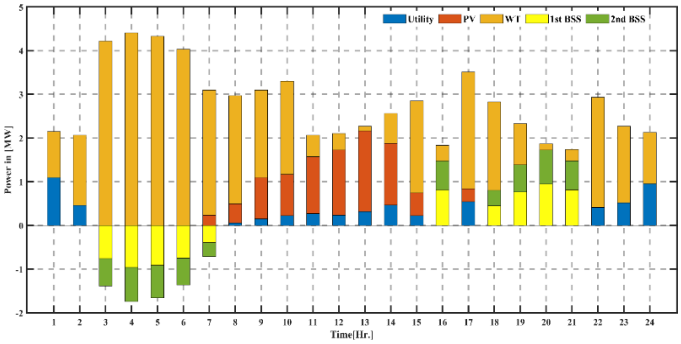

Figure 15. Hourly Optimal Output Power of PV, WT, BSS, and Utility

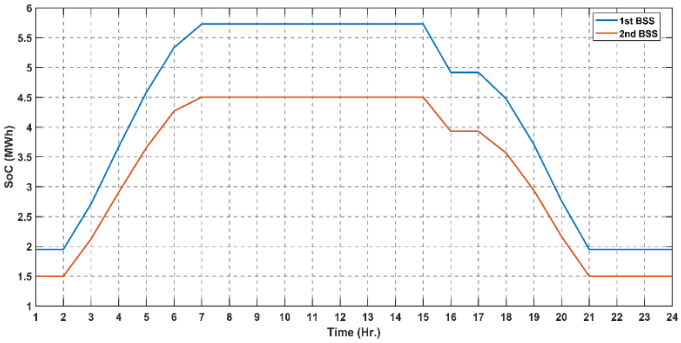

Figure 16. State of Charge of the Two-BSS Configuration Using the WO Algorithm

The proposed WO-based approach provides significant scalability and generality, as the adopted power flow model, battery operating constraints, and optimization structure are adaptable to larger distribution networks through system-specific adjustments. Furthermore, while the optimization method is constrained to BSS design variables, the corresponding computational demand remains acceptable, maintaining the framework's relevance and efficiency for extensive power systems.

7. CONCLUSION

This research proposes an effective allocation of BSSs within the MG by utilizing the WO optimizer. This optimal design improves the objective function in terms of power loss reduction. This, in turn, facilitates MG performance assessment, enhances voltage stability and profiles, aligns RERs with capacity ratings for optimal integration, and enables peak shifting to minimize operational expenses during power transfer. The six proposed methodologies—GA, PSO, SSLO, I-GWO, DBA, and WO—are employed to demonstrate that WO efficiently schedules double BSS power flow. MG power losses are reduced by 53.56%, resulting in a maximum operational cost saving of 10.74%. The improved voltage profile elevates the weakest voltage node to 0.9803 p.u. The minimum VSI is attained as 1.01821 p.u. The results indicate that WO-based double BSS planning enhances MG reliability by accelerating convergence, improving computational efficiency, ensuring balanced exploration and exploitation, and avoiding local optima due to its strong search capability and low objective variance. The consistency and suitability of WO in MG applications are confirmed.

Author Contributions: Conceptualization, H.A. and S.H.; methodology, H.A., M.D, and S.H; software, H.A. and M.D.; validation, H.A., S.H. and M.D.; formal analysis, H.A., S.H. and M.D.; investigation, H.A., S.H. and M.D; resources, H.A and M.D.; data curation, H.A., S.H. and M.D; writing—original draft preparation, H.A., S.H. and M.D; writing—review and editing, S.H. and M.D; visualization, H.A., S.H. and M.D; supervision, S.H.; project administration, H.A., S.H. and M.D; funding acquisition, H.A., S.H. and M.D. All authors have read and agreed to the published version of the manuscript.

Funding: This research received no external funding.

Conflicts of Interest: The funders had no role in the design of the study; in the collection, analyses, or interpretation of data; in the writing of the manuscript, or in the decision to publish the results.

REFERENCES

[1] S. Dawn et al., "Integration of Renewable Energy in Microgrids and Smart Grids in Deregulated Power Systems: A Comparative Exploration," Adv. Energy Sustain. Res., vol. 5, no. 10, Oct. 2024, doi: 10.1002/aesr.202400088.

[2] M. Hamidieh and M. Ghassemi, "Microgrids and Resilience: A Review," 2022, Institute of Electrical and Electronics Engineers Inc. doi: 10.1109/ACCESS.2022.3211511.

[3] Y. Shang, D. Han, G. Gozgor, M. K. Mahalik, and B. K. Sahoo, "The impact of climate policy uncertainty on renewable and non-renewable energy demand in the United States," Renew. Energy, vol. 197, pp. 654–667, Sep. 2022, doi: 10.1016/j.renene.2022.07.159.

[4] Chijioke Paul Agupugo, Husseini Musa Kehinde, and Helena Nbéu Nkula Manuel, "Optimization of microgrid operations using renewable energy sources," Eng. Sci. Technol. J., vol. 5, no. 7, pp. 2379–2401, Jul. 2024, doi: 10.51594/estj.v5i7.1360.

[5] D. A. Elalfy, E. Gouda, M. F. Kotb, V. Bureš, and B. E. Sedhom, "Comprehensive review of energy storage systems technologies, objectives, challenges, and future trends," Energy Strateg. Rev., vol. 54, p. 101482, Jul. 2024, doi: 10.1016/j.esr.2024.101482.

[6] M. Gholami, S. M. Muyeen, and S. Lin, "Optimizing microgrid efficiency: Coordinating commercial and residential demand patterns with shared battery energy storage," J. Energy Storage, vol. 88, May 2024, doi: 10.1016/j.est.2024.111485.

[7] T. Kerdphol, K. Fuji, Y. Mitani, M. Watanabe, and Y. Qudaih, "Optimization of a battery energy storage system using particle swarm optimization for stand-alone microgrids," Int. J. Electr. Power Energy Syst., vol. 81, pp. 32–39, 2016, doi: 10.1016/j.ijepes.2016.02.006.

[8] M. V. T. Khanh Trinh, "Research On Genetic Algorithms: Concepts, Models, And Applications," Int. J. Educ. Soc. Sci. Res., vol. 08, no. 03, pp. 354–373, 2025, doi: 10.37500/IJESSR.2025.8324.

[9] S. P. Collins et al., "Techno-Economic Analysis Of Off-Grid Hybrid Pv-Diesel-Battery System In Katsina State, Nigeria," Arid Zo. J. Eng. Technol. Environ., Vol. 14, No. 2, Pp. 167–186, 2021.

[10] P. Tozzi and J. H. Jo, "A comparative analysis of renewable energy simulation tools: Performance simulation model vs. system optimization," Renew. Sustain. Energy Rev., vol. 80, no. August 2016, pp. 390–398, 2017, doi: 10.1016/j.rser.2017.05.153.

[11] H. A. Kazem, T. Khatib, and K. Sopian, "Sizing of a standalone photovoltaic/battery system at minimum cost for remote housing electrification in Sohar, Oman," Energy Build., vol. 61, no. March 2013, pp. 108–115, 2013, doi: 10.1016/j.enbuild.2013.02.011.

[12] S. Saremi, S. Mirjalili, and A. Lewis, "Grasshopper Optimisation Algorithm: Theory and application," Adv. Eng. Softw., vol. 105, pp. 30–47, 2017, doi: 10.1016/j.advengsoft.2017.01.004.

[13] T. Kerdphol, Y. Qudaih, and Y. Mitani, "Optimal Battery Energy Storage Size Using Particle Swarm Optimization for Microgrid System," Int. Rev. Electr. Eng., vol. 10, no. 2, p. 277, Apr. 2015, doi: 10.15866/iree.v10i2.5350.

[14] N. Skunana, "Optimal Placement of Battery Energy Storage System for Voltage Profile Improvement and Reduction of Power Losses," 2025 33rd South. African Univ. Power Eng. Conf., pp. 1–6, 2025, doi: 10.1109/SAUPEC65723.2025.10944322.

[15] K. Kaiyawong, C. Plongkrathoke, and K. Chayakulkheeree, "Bi-level Planning Model for Optimal Battery Energy Storage Allocation Considering Optimal Daily Scheduling Using Mixed-Integer Particle Swarm Optimization," Eng. J., vol. 27, no. 8, pp. 13–27, Aug. 2023, doi: 10.4186/ej.2023.27.8.13.

[16] X. Feng, J. Gu, and X. Guan, "Optimal allocation of hybrid energy storage for microgrids based on multi-attribute utility theory," J. Mod. Power Syst. Clean Energy, vol. 6, no. 1, pp. 107–117, 2018, doi: 10.1007/s40565-017-0310-3.

[17] S. Sharma, S. Bhattacharjee, and A. Bhattacharya, "Grey wolf optimisation for optimal sizing of battery energy storage device to minimise operation cost of microgrid," IET Gener. Transm. Distrib., vol. 10, no. 3, pp. 625–637, Feb. 2016, doi: 10.1049/iet-gtd.2015.0429.

[18] S. Garip and S. Ozdemir, "Optimization of PV and Battery Energy Storage Size in Grid-Connected Microgrid," Appl. Sci., vol. 12, no. 16, p. 8247, Aug. 2022, doi: 10.3390/app12168247.

[19] L. A. Wong, V. K. Ramachandaramurthy, S. L. Walker, P. Taylor, and M. J. Sanjari, "Optimal placement and sizing of battery energy storage system for losses reduction using whale optimization algorithm," J. Energy Storage, vol. 26, no. May, p. 100892, Dec. 2019, doi: 10.1016/j.est.2019.100892.

[20] F. Mohamad, J. Teh, and C. M. Lai, "Optimum allocation of battery energy storage systems for power grid enhanced with solar energy," Energy, vol. 223, 2021, doi: 10.1016/j.energy.2021.120105.

[21] T. Boonraksa, W. Pinthurat, P. Wongdet, P. Boonraksa, B. Marungsri, and B. Hredzak, "Optimal Capacity and Cost Analysis of Hybrid Energy Storage System in Standalone DC Microgrid," IEEE Access, vol. 11, pp. 65496–65506, 2023, doi: 10.1109/ACCESS.2023.3289821.

[22] A. A. Hassan and D. M. Atia, "Optimizing microgrid integration of renewable energy for sustainable solutions in off/on-grid communities," J. Electr. Syst. Inf. Technol., vol. 11, no. 1, p. 61, Dec. 2024, doi: 10.1186/s43067-024-00186-6.

[23] P. Gao, H. Chen, and X. Wu, "Optimal planning of energy storage systems in active distribution networks considering multiple operation optimisation measures," CIRED - Open Access Proc. J., vol. 2020, no. 1, pp. 4–8, 2020, doi: 10.1049/oap-cired.2021.0005.

[24] M. H. Moradi and M. Abedini, "A novel method for optimal DG units capacity and location in Microgrids," Int. J. Electr. Power Energy Syst., vol. 75, pp. 236–244, 2016, doi: 10.1016/j.ijepes.2015.09.013.

[25] M. Lehtonen, "Enhancing Renewable Energy Hosting Capacity in Unbalanced Microgrids via Empowering Smart Inverters," IEEE Access, vol. 13, no. January, pp. 17161–17181, 2025, doi: 10.1109/ACCESS.2025.3533043.

[26] J. Liao, J. Lin, and G. Wu, "Two-layer optimization configuration method for distributed photovoltaic and energy storage systems based on IDEC-K clustering," Energy Reports, vol. 11, no. April, pp. 5172–5188, 2024, doi: 10.1016/j.egyr.2024.04.047.

[27] Z. Wang, Y. Gao, and Y. Gao, "Optimization of Distributed Photovoltaic Energy Storage System Double-Layer Planning in Low-Carbon Parks Considering Variable Operating Conditions and Complementary Synergy of Energy Storage Devices," 2025, doi: 10.3390/en18081881.

[28] J. Ye, "Knowledge-Based Systems Stochastic social learning optimization : Combining social learning and bucket theory for efficient optimization," Knowledge-Based Syst., vol. 341, no. March, p. 115767, 2026, doi: 10.1016/j.knosys.2026.115767.

[29] Jun Cheng, Wim De Waele, "Detective Behavior Algorithm (DBA): A New Metaheuristic for Design and Engineering Optimization," vol. 338, no. 0950-7051,, doi: 1016/j.knosys.2026.115434.

[30] S. Khunkitti, P. Boonluk, and A. Siritaratiwat, "Optimal Location and Sizing of BESS for Performance Improvement of Distribution Systems with High DG Penetration," Int. Trans. Electr. Energy Syst., vol. 2022, 2022, doi: 10.1155/2022/6361243.

[31] S. Zanoni and B. Marchi, "Optimal Sizing of Energy Storage Systems for Industrial Production Plants," IFIP Adv. Inf. Commun. Technol., vol. 439, no. PART 2, pp. 342–350, 2014, doi: 10.1007/978-3-662-44736-9_42.

[32] E. Jacob and H. Farzaneh, "Modeling and performance evaluation of hybrid photovoltaic thermal, wind, and battery microgrids using optimization and dynamic simulation," Sci. Rep., vol. 15, no. 1, pp. 1–28, 2025, doi: 10.1038/s41598-025-95149-w.

[33] J. Jung, K. Baek, E. Lee, W. Ko, and J. Kim, "Economic Analysis of Special Rate for Renewable Energy Based on the Design of an Optimized Model for Distributed Energy Resource Capacities in Buildings," Energies, vol. 14, no. 3, p. 645, Jan. 2021, doi: 10.3390/en14030645.

[34] T. Kerdphol, K. Fuji, Y. Mitani, M. Watanabe, and Y. Qudaih, "Optimization of a battery energy storage system using particle swarm optimization for stand-alone microgrids," Int. J. Electr. Power Energy Syst., vol. 81, no. October, pp. 32–39, 2016, doi: 10.1016/j.ijepes.2016.02.006.

[35] K. N. Ukoima, O. I. Okoro, U. B. Akuru, and I. E. Davidson, "Determination of the Weibull parameters and wind power potential: A case of Okorobo-Ile town, Rivers state, Nigeria," Wind Energy Eng. Res., vol. 2, no. November, p. 100006, 2024, doi: 10.1016/j.weer.2024.100006.

[36] M. Hosseina, M. S. Moghaddam, and A. Hassannia, "Optimizing energy and load management in island microgrids for enhancing resilience against resource interruptions," Sci. Rep., vol. 15, no. 1, pp. 1–25, 2025, doi: 10.1038/s41598-025-99974-x.

[37] P. Nikolaidis and A. Poullikkas, "A comparative review of electrical energy storage systems for better sustainability," J. Power Technol., vol. 97, no. 3, pp. 220–245, 2011.

[38] D. Wang, J. Qiu, L. Reedman, K. Meng, and L. L. Lai, "Two-stage energy management for networked microgrids with high renewable penetration," Appl. Energy, vol. 226, pp. 39–48, Sep. 2018, doi: 10.1016/j.apenergy.2018.05.112.

[39] S. Ahmed, "Energy Storage Systems : Scope , Technologies , Characteristics , Progress , Challenges , and Future Suggestions — Renewable Energy Community Perspectives," pp. 1–32, 2025, doi: 10.3390/en18112679.

[40] S. S. Kanojia and B. N. Suthar, "Voltage stability index : a review based on analytical method , formulation and comparison in renewable dominated power system," vol. 13, no. 2, pp. 508–520, 2024, doi: 10.11591/ijape.v13.i2.pp508-520.

[41] M. Chakravorty and D. Das, "Voltage stability analysis of radial distribution networks," Int. J. Electr. Power Energy Syst., vol. 23, no. 2, pp. 129–135, Feb. 2001, doi: 10.13140/2.1.1729.8884 CITATION.

[42] M. H. Mostafa, S. H. E. A. Aleem, S. G. Ali, A. Y. Abdelaziz, S. Member, and P. F. Ribeiro, "Robust Energy Management and Economic Analysis of Microgrids Considering Different Battery Characteristics," IEEE Access, vol. PP, p. 1, 2020, doi: 10.1109/ACCESS.2020.2981697.

[43] G. A. Setia, G. HM Sianipar, K. Samudra, F. Haz, N. Winanti, and H. R. Iskandar, "Implementation of Backward-Forward Sweep Method on Load Model Variation of Distribution Systems," in 2019 2nd International Conference on High Voltage Engineering and Power Systems (ICHVEPS), IEEE, Oct. 2019, pp. 1–5. doi: 10.1109/ICHVEPS47643.2019.9011141.

[44] P. Trojovský and M. Dehghani, "Walrus Optimization Algorithm: A New Bio-Inspired Metaheuristic Algorithm," Oct. 24, 2022, Scientific Reports. doi: 10.21203/rs.3.rs-2174098/v1.

[45] M. Aicha, B. Lamia, L. Salima, and B. Ibtissam, "Optimal Energy Management of a Microgrid Using Walrus Optimizer Algorithm," vol. 12, no. 1, pp. 362–370, 2026, doi: 10.22399/ijcesen.4785.

[46] H. M. Hasanien, I. Alsaleh, Z. Ullah, and A. Alassaf, "Probabilistic optimal power flow in power systems with Renewable energy

International Journal of
Electrical and Electronics Research (IJEER)
Research Article | Volume 14, Issue 2 | Pages 526-541 | e-ISSN: 2347-470X

integration using Enhanced walrus optimization algorithm," Ain Shams Eng. J., vol. 15, no. 3, p. 102663, Mar. 2024, doi: 10.1016/j.asej.2024.102663.

[47] H. M. Sultan, M. A. Mossa, and A. Y. Abdelaziz, "Parameter Identification of Solar Cell Mathematical Models Using Metaheuristic Algorithms," in Advances in Solar Photovoltaic Energy Systems, IntechOpen, 2024. doi: 10.5772/intechopen.1004044.

[48] D. Sanin-Villa, H. A. Figueroa-Saavedra, and L. F. Grisales-Noreña, "Efficient BESS Scheduling in AC Microgrids via Multiverse Optimizer: A Grid-Dependent and Self-Powered Strategy to Minimize Power Losses and CO2 Footprint," Appl. Syst. Innov., vol. 8, no. 3, p. 85, Jun. 2025, doi: 10.3390/asi8030085.

[49] T. Oluwaseun, S. Vincent, M. Josephine, and O. Anthony, "Walrus optimizer algorithm for techno-economic modeling of an autonomous hybrid microgrid energy management system," Energy Convers. Manag., vol. 344, no. August, p. 120277, 2025, doi: 10.1016/j.enconman.2025.120277.

[50] V. A. Cicirello and S. F. Smith, "Modeling GA Performance for Control Parameter Optimization," no. July, 2013.

[51] Y. Qiu, X. Yang, and S. Chen, "An improved gray wolf optimization algorithm solving to functional optimization and engineering design problems," Sci. Rep., pp. 1–25, 2024, doi: 10.1038/s41598-024-64526-2.

[52] T. M. Shami, A. A. El-Saleh, M. Alswaitti, Q. Al-Tashi, M. A. Summakieh, and S. Mirjalili, "Particle Swarm Optimization: A Comprehensive Survey," IEEE Access, vol. 10, pp. 10031–10061, 2022, doi: 10.1109/ACCESS.2022.3142859.

© 2026 by Hager A. Elwelily, Sayed H. A. El-Banna, and Mahmoud A. El-Dabah. Submitted for possible open access publication under the terms and conditions of the Creative Commons Attribution (CC BY) license (http://creativecommons.org/licenses/by/4.0/).